

Assessment of Multispectral Vegetation Features for Digital Terrain Modeling in Forested Regions

Tito Arevalo-Ramirez^{ID}, Javier Guevara^{ID}, Member, IEEE, Robert Guaman Rivera^{ID}, Juan Villacrés^{ID}, Oswaldo Menéndez^{ID}, Member, IEEE, Andrés Fuentes, and Fernando Auat Cheein^{ID}, Senior Member, IEEE

Abstract—Bare-earth extraction in forested regions has been considered challenging because of the lack of ground point information. In these regions, vision systems cannot capture any information about ground points under the canopy. Thus, the challenge of generating a digital terrain model by cameras increases. Nevertheless, one might alleviate ground filtering using vegetation's features (e.g., chlorophyll). In this regard, this article evaluated two machine-learning approaches [i.e., conditional random field (CRF), artificial neural network (ANN)] for generating digital terrain models when biophysical or biochemical features of vegetation are given. Terrain models were generated from multispectral image-based point clouds. A fivefold cross-validation methodology evaluated the CRF and ANN. The point clouds were retrieved from two study areas at different illumination and flight altitudes. Vegetation features were computed as vegetation indices from the multispectral point clouds. Results suggested that by using these indices, the classification of ground points could be enhanced. In particular, the vegetation indices that yielded the best outcomes were normalized difference vegetation index, green NDVI, and modified chlorophyll absorption reflectance index. Moreover, it was shown that CRF generates elevation models more smoothly than a triangular irregular network method. Thus, a CRF could be promising for classifying ground points in forested regions using geometric and vegetation features from a photogrammetric point cloud.

Index Terms—Conditional random field (CRF), digital terrain model, multispectral, vegetation indices.

I. INTRODUCTION

IN THE last five years, Maule, a central region in Chile, has been threatened continuously by wildfires. Indeed, it has become one of the regions most damaged by wildfires with about 57 000 burned hectares per year [1]. In this context, the main factors influencing the susceptibility of the zone to fire are its Mediterranean climate, vegetation, and

Manuscript received April 21, 2021; revised July 9, 2021; accepted August 19, 2021. Date of publication September 15, 2021; date of current version January 21, 2022. This work was supported in part by the Agencia Nacional de Investigación y Desarrollo (ANID)/PFCHA/DOCTORADO NACIONAL CHILE under Grant 2019-21190471, Grant /2020-21200684, Grant/2020-21200700, Grant FONDECYT 1201319, and Grant PIA/ANILLO ACT172095; in part by the Advance Center of Electrical and Electronic Engineering under Grant AC3E FB0008; and in part by PIIC 2021/1, DGIIP-UTFSM Chile. (Corresponding author: Fernando Auat Cheein.)

Tito Arevalo-Ramirez, Javier Guevara, Robert Guaman Rivera, Juan Villacrés, Oswaldo Menéndez, and Fernando Auat Cheein are with the Department of Electronics, Universidad Técnica Federico Santa María, Valparaíso 2390123, Chile (e-mail: fernando.autat@usm.cl).

Andrés Fuentes is with the Department of Industries, Universidad Técnica Federico Santa María, Valparaíso 2390123, Chile.

Digital Object Identifier 10.1109/TGRS.2021.3109601

topography [2]. Therefore, to avoid potential fires, there is a need to determine the areas (e.g., forested areas) with higher risk before the fire reaches them. However, the prevention, detection, and response to wildfires present a challenging task because of Maule's topographical and urban features [3].

To determine susceptible areas, one can be supported by risk-based tools that employ bare-earth models. Specifically, these models are related to fire behavior because of the relationship between terrain morphology, fire severity, and spreading [4]. Information about bare-earth, that is, digital terrain model (DTM), is widely used in many study fields to classify and assess the objects above the ground [5]. In general, DTMs are obtained by an interpolation method after identifying ground points from a point cloud. The reader can find details about the state-of-the-art process to generate DTMs (ground filtering methods) in [6], and references therein. However, developing DTMs in forest regions is not an easy task. Specifically, information about terrain is sparse because forest canopy hinders remote-sensing platforms from capturing terrain data [7].

Despite the difficulties faced in forested regions, remote-sensing platforms, under certain conditions, are capable of retrieving enough information to generate DTMs. LiDAR sensors (i.e., full-waveform and multireturn systems) are the most suitable for these scenarios because they are active sensors [7]. In particular, LiDAR systems can penetrate the forest canopy and record information about the terrain surface. Yet, data recording can be limited by canopy density [8]. On the other side, although vision systems are passive sensors, they can also record information about the terrain. One can extract the bare-earth model after generating an image-based point cloud [9]. To obtain a DTM by an image-based point cloud, it is common to use ground filtering algorithms initially developed for LiDAR sensors [10].

When vision systems record enough information about bare-earth surfaces, the differences between a DTM extracted from image-based or LiDAR point clouds are minimal [11]. In particular, Jensen and Mathews [11] showed that terrain elevation is overestimated by the DTM generated from image-based point cloud. The average difference is about 0.19 m with a standard deviation of 0.66 m. It is worth to mention that most of the differences take place in forested areas. Jensen and Mathews [11] used as reference a bare-earth model generated from the LiDAR point cloud. On the other side,

Meng *et al.* [12] proposed an object-oriented classification ensemble algorithm to improve landscape classification and terrain estimation in wetlands. The proposed method improved the height RMSE from 0.342 to 0.177 m in low vegetation and 1.305 to 0.057 m in tall vegetation. However, their method requires field GPS surveys, which are not suitable in all mapping areas, such as in [13]. Furthermore, Graham *et al.* [10] found that one could extract an acceptable DTM from an image-based point cloud when, on average, the canopy surface is lower than 70%. Graham *et al.* [10] accomplished a height RMSE less than 1.5 m in the 57% of the terrain by determining the optimal parameters of three ground filtering methods (progressive triangular irregular network densification, hierarchical robust interpolation, and simple progressive morphological filtering).

The works mentioned above show that image-based point clouds are suitable for generating DTMs. Nevertheless, we believe that ground classification accuracy can be improved by adding forest features. We posit that canopy features, retrieved by a multispectral camera, could bring latent information about forest and terrain features. Thus, algorithms might discriminate better ground points by including such features in the bare-earth identification process. This idea is also stated in [6], which suggests that features of multisources can enhance the ground filtering algorithm (e.g., LiDAR and vision system). For instance, Gilani *et al.* [14] has merged multispectral and LiDAR data to advance classification tasks; however, they are not focused on generating a DTM perse.

Anders *et al.* [15] merged the output of two different ground filtering methods to improve digital terrain modeling. Specifically, they used an iterative surface lowering and excessive greenness index-based methods (ISL-EGI). Results showed that ISL-EGI did not overcome the DTM performed by a triangular irregular network method. The lower performance of ISL-EGI was attributed to the standard RGB camera used to capture vegetation features [15].

Regarding our approach, it is inspired on the works proposed in [5] and [16]. Both works used a probabilistic framework based on conditional random field (CRF) to classify ground and nonground points. In particular, Niemeyer *et al.* [5] used full-waveform LiDAR to yield the study site point cloud and label its points as ground, buildings, and vegetation. Despite the overall accuracy (94%), Niemeyer *et al.* [5] computed a LiDAR point feature vector based on a prior bare-earth model (i.e., distance to the ground). This work is focused on point cloud classification tasks rather than terrain modeling.

Conversely, Lu *et al.* [16] aimed to infer the bare-earth elevation from a multi return LiDAR-based point cloud by a hybrid CRF. The proposed method jointly employs a CRF and a Gaussian random field (GRF) to classify and estimate ground points' elevation. Nevertheless, Lu *et al.* [16] did not use vegetation features of the vegetation to improve the classification nor photogrammetric point cloud. Furthermore, assume conditional independence between the point labels, which might not be ignored when introducing vegetation features.

In this context and to improve the generation of DTMs, we evaluate the integration of vegetation features for bare-earth

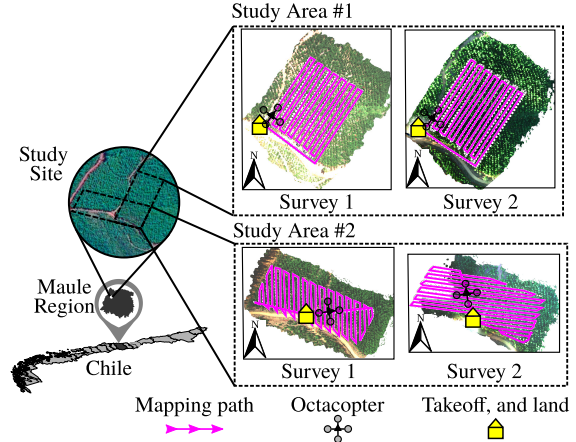


Fig. 1. Location of the study site. The study site is located in Maule region. MicaSense Red-edge camera captured multispectral images of each study area.

TABLE I
Pinus Insigne FOREST METRICS. THE DATA WAS PROVIDED BY THE FOREST MANAGER. DBH REFERS TO DIAMETER AT BREAST HEIGHT, AND STD IS THE STANDARD DEVIATION

	Height (cm)	DBH (mm)	Basal areal ($m^2 ha^{-1}$)	Biomass ($m^3 ha^{-1}$)
Average	495.8	79.16	5.781	29.84
Std	50.92	8.902	3.314	20.28

modeling in forested regions. To this aim, we exploit the potential of CRF, an artificial neural network (ANN) to classify ground points, and GRF to infer ground point elevation. Note that the ANN model is used to compare the CRF results. We consider the point cloud as a probabilistic graphical model where each point represents a graph node. Each node is then associated with discrete and continuous random variables to assess each point's label and elevation, respectively. Vegetation indices are integrated into the classification step as point features. Then, the height of the ground points is estimated, and DTM is generated.

This work is organized as follows: Section II shows a description of the study site, instruments, and data processing. The proposed methodology is shown in Section III. Results and discussions are presented in Sections IV and V, respectively. Finally, Section VI exposes the conclusions.

II. DATA ACQUISITION

Point cloud of the study site was obtained by remotely piloted aircraft (RPA) surveys in the Maule region ($35^{\circ}13'14.2''S + 72^{\circ}09'27.4''W$), as shown in Fig. 1. The climate of this region can be characterized as Mediterranean temperate. On average, Maule's temperature is about $19^{\circ}C$ with precipitations that can soar up to 758 mm [17]. The study site is a six-year-old *Pinus insigne* forest plantation and native shrubs. Pine forest metrics are described in Table I. Native shrubs' height is lower than 1 m. From the study site, we selected two study areas to be mapped. Both study areas were about $10\,000\,m^2$. Study areas and flight parameters were selected according to the guidelines described in [18].

A. Field Surveys

We mapped the study areas using a MicaSense RedEdge camera (MicaSense RedEdge—M, MicaSense Inc., Seattle, USA) mounted on a nadir position on a Tarot T-18 octocopter (Tarot T-18, UAV Systems International, Houston, USA). The multispectral camera allowed recording images in five spectral bands: blue (475 nm), green (560 nm), red (668 nm), red-edge (717), near-infrared (840). The flight speed, altitude, and lateral distance for each study area are set as follows: study area #1, 5 ms⁻¹, 40 m, and 6.67 m; study area #2, 4 ms⁻¹, 30 m, and 6 m.

For each study area, two mapping surveys at different times were performed. We mapped the study area #1 at 13:00 and 19:20 GMT-4 on November 21, 2020, and study area #2 at 16:38 and 19:38 GTM-4 on November 22, 2020 (see Fig. 1). Note that for study area #2, the drone performed a different path for each survey because of wind direction.

B. Data Processing

Agisoft Metashape Professional software (<https://www.agisoft.com/>) implements a structure from motion algorithm to retrieve the 3-D information from a scene [19]. Following the workflow detailed in [19], Agisoft performed a radiometric calibration of the recorded images. The radiometric calibration allows converting raw pixel values (digital number) into absolute spectral radiance values. Details about radiometric calibration can be found in [20]. Note that each image stores the parameters required for radiometric correction in its metadata field. However, images from a reference panel are required to calibrate the reflectance values properly. Reference panel images should be captured immediately before and after the flight survey.

Next, images are aligned and the matching points between the images generate the point cloud. In brief, the workflow for processing the images and building the point clouds is as follows: To perform a radiometric calibration, to align the images, and to generate the point cloud. All this workflow is implemented by Agisoft software and is straight to follow (see [19]).

It is important to remark that we use two-parameter setup for generating point clouds at different quality. Specifically, the high-quality point clouds are generated as follows: to align photos with high *accuracy*, 60 000 *key point limit*, and 6000 *tie point limit*; to build dense cloud with ultrahigh *quality*, *reuse depth map* true, *calculate point color* true, and *calculate point confidence* true. On the other side, lower quality point clouds are generated using Agisoft default parameters and *depth filtering* aggressive. Text in italic refers to Agisoft parameters.

Regarding class labels ground truth, we use the MATLAB toolbox simple morphological filter (SMRF) to automatically separate ground points and nonground points (i.e., trees, cars, and people). The labeled point cloud (terrain and forest labels) is generated by manual adjustment of SMRF parameters [21]. Next, we relabel the misclassified points manually using Cloud compare software (<https://www.danielgm.net/cc/>). Moreover, the bare-earth height reference model is generated by LAStools software (<https://rapidlasso.com/lastools/>) [22].

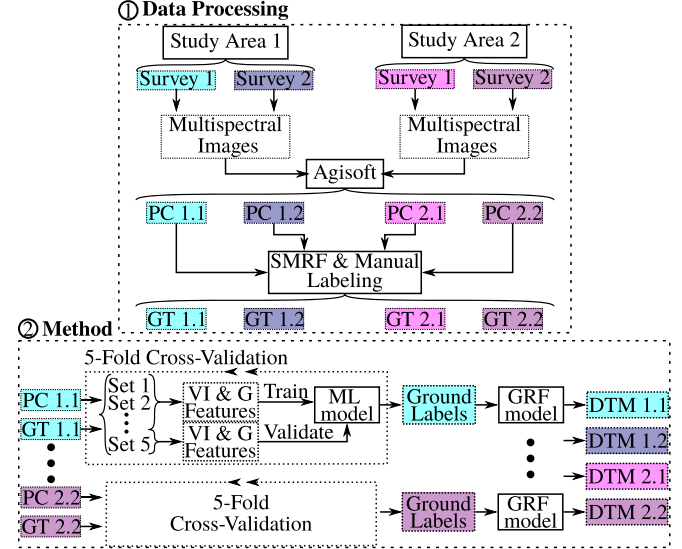


Fig. 2. General architecture for modeling terrain in forested regions by CRF, ANN, and GRF models. Where PC X.Y refers to the Point Cloud generated from the study area #X using the data of the survey Y; GT is the point cloud labels ground truth; VI are the multispectral vegetation indices; G are the point cloud geometric features; ML refers to machine learning models (CRF, ANN).

TABLE II

QUANTITATIVE METRICS FOR EVALUATING THE PERFORMANCE OF CRF.
WHERE OM IS THE OMISSION ERROR, COM IS COMMISSION ERROR,
 e_{TOTAL} IS THE TOTAL ERROR, AND ACC IS THE
CLASSIFICATION ACCURACY

		Predicted		Errors	
Ground-truth	ground	ground	non-ground	om = b/(a + b)	com = c/(c + d)
	non-ground	a	b	$e_{\text{total}} = (b + c)/(a + b + c + d)$	$acc = (a + d)/(a + b + c + d)$

III. METHODS

Once the multispectral images were processed and generated the point clouds, we extract ground points by a CRF and ANN methods and then estimate ground points elevation under canopy using an intrinsic GRF [16]. These models are implemented in MATLAB code using the CRF and deep learning toolboxes. The former is developed by Schmidt [23] and the latter is included in MATLAB software. Specifically, we evaluate the classification models by a fivefold cross-validation methodology. To this aim, the point clouds are divided into five sets. Next, for each set, vegetation and geometric features are computed. Then, CRF and ANN models are trained using four sets and validated with the remaining. This procedure is repeated up to the models are validated with all sets. Classification performance is assessed using the metrics listed in Table II. After the point cloud ground labels are determined, the elevation of points under the canopy is inferred by the GRF. Fig. 2 shows the general scheme for classifying ground points.

A. Machine Learning Methods

CRF is a probabilistic framework that allows performing contextual classification [24]. In general, CRF is assembled

TABLE III

VEGETATION INDICES USED TO CHARACTERIZE THE VEGETATION, WHERE ρ_a IS THE REFLECTANCE IN THE a BAND, B IS THE BLUE CHANNEL, G IS THE GREEN CHANNEL, R IS THE RED CHANNEL, RE IS THE RED-EDGE CHANNEL, AND NIR IS THE NEAR-INFRARED CHANNEL

Vegetation Indices	Equations	Reference
Normalized Difference Vegetation Index (NDVI)	$\frac{\rho_{NIR} - \rho_R}{\rho_{NIR} + \rho_R}$	[28]
Green Normalized Difference Vegetation Index (GNDVI)	$\frac{\rho_{NIR} - \rho_G}{\rho_{NIR} + \rho_G}$	[29]
Modified Soil Adjusted Vegetation Index (MSAVI)	$\frac{2\rho_{NIR} + 1 - \sqrt{2\rho_{NIR} + 1 - 8(\rho_{NIR} - \rho_R)}}{2}$	[30]
Optimization of Soil Adjusted Vegetation Index (OSAVI)	$\frac{1.16(\rho_{NIR} - \rho_R)}{\rho_{NIR} + \rho_R + 0.16}$	[31]
Enhanced Vegetation Index (EVI)	$2.5 \frac{\rho_{NIR} - \rho_R}{\rho_{NIR} + 6\rho_R - 7.5\rho_B + 1}$	[32]
Chlorophyll Absorption Reflectance Index (CARI)	$(\rho_{RE} - \rho_R) - 0.2(\rho_{RE} - \rho_G)$	[33]
Modified CARI (MCARI)	$\frac{\rho_{RE}(\rho_{RE} - \rho_R) - 0.2(\rho_{RE} - \rho_G)}{\rho_{NIR} - \rho_{RE}}$	[34]
Red Edge Normalized Difference Vegetation Index (RENDVI)	$\frac{\rho_{NIR} - \rho_{RE}}{\rho_{NIR} + \rho_{RE}}$	[29]
Red Edge Modified Simple Ratio (REMSR)	$\frac{\rho_{NIR}/\rho_{RE} - 1}{\sqrt{\rho_{NIR}/\rho_{RE} + 1}}$	[35]

by a set of nodes and a set of edges. For each node, one can associate a discrete random variable for denoting the node's class label. The edges show the probabilistic relationship between nodes. Details about CRF implementation can be found in [16] and [23]. In particular, each point of the point cloud is considered as a CRF node, and CRF edges were determined using a 3-D Delaunay triangulation [25].

Despite ANNs are commonly used for solving image-based problems, they have appealing advantages for remote-sensing processing applications [26]. In this regard, we implemented an ANN using two hidden layers. The first was built using 100 neurons and a relu function for activation. The second consisted of two neurons and a softmax activation function. The data forward propagated through the input layer was normalized by subtracting the mean and dividing by the standard deviation.

To determine the elevation of ground points under the forest canopy, we implemented a GRF algorithm proposed in [16]. This algorithm estimates ground point elevations by an expectation–maximization procedure. To this aim, the GRF method should know the point label (ground or nonground). Implementation details are shown in [16].

B. Input Features

The vegetation and geometric features employed to determine the DTM are described as follows.

1) *Vegetation Features:* Vegetation features are estimated using multispectral vegetation indices. Table III shows the vegetation indices that were used in this work. We chose these indices because they have been used in forest tree classification and precision agriculture [27]. The VIs were computed using the point color information that is available in four bands (i.e. R, G, B, NIR, RE).

2) *Geometric Features:* We make use of the point-slope, curvature, and segmented-based features. Because of space limitations, we refer the reader to CRF feature assessment from [25] for a more detailed description.

C. Training

The CRF and ANN models were evaluated using a five-fold cross-validation setup with 11 input vector sets and

TABLE IV

INPUT VECTOR SETS

Set 1 Geometric	Set 2 Geometric & NDVI	Set 3 Geometric & GNDVI	Set 4 Geometric & MSAVI	Set 5 Geometric & OSAVI	Set 6 Geometric & EVI
Set 7 Geometric & CARI	Set 8 Geometric & MCARI	Set 9 Geometric & RENDVI	Set 10 Geometric & REMSR	Set 11 Geometric & All VIs	

TABLE V

DESCRIPTION OF THE GENERATED POINT CLOUDS FROM BOTH STUDY AREAS USING AGisoft SOFTWARE

Study Area	GTM-4 Time	Quality	Point Clouds		
			Size	Nonground %	Ground %
1	13:00	High	66500	54.77	45.23
		Low	62360	71.08	28.92
	19:20	High	53896	85.62	14.38
		Low	62721	82.82	17.18
2	16:38	High	109078	71.40	28.60
		Low	109995	78.74	21.26
	19:38	High	120570	73.20	26.80
		Low	122303	85.99	14.01

TABLE VI

SUMMARY OF CROSS-VALIDATION RESULTS. DETAILED DESCRIPTION OF QUANTITATIVE METRICS ARE SHOWN IN TABLE VIII

	CRF				ANN			
	om	com	e_{total}	acc	om	com	e_{total}	acc
Average	16.6	11.5	12.6	87.4	28.1	10.6	13.6	86.4
STD	8.90	3.02	2.90	2.90	11.3	9.15	6.10	6.10

compare the classification performance of each one. The input vector sets are described in Table IV. In particular, we trained each CRF using the Loopy belief propagation method. Optimal model parameters were estimated using a quasi-Newton method (i.e., L-BFGS). Furthermore, we use maximum posterior criteria to choose the point labels. The reader can find more details about training in [23]. Regarding the ANN, it was trained using ADAM optimization algorithm.

IV. RESULTS

By two RPA surveys per day of both study areas, we generated four photogrammetric-based point clouds (at high and low quality). The point clouds are described in Table V. To ease the results visualization, from this point forward, we label the point clouds as follows: PC X.Y, where PC refers to point cloud, X is the study area, Y corresponds to the survey of the day, and Q the point cloud quality. Thus, PC 1.2-H is the label for the point cloud from the first study area using the data recorded by the second survey (19:20 GTM-4) and generated at high quality.

The CRF and ANN cross-validation results are summarized in Table VI (see Table VIII for detailed results). We found that vegetation indices might add information to better discriminate ground and canopy points. In general, the classification accuracy is increased by using VIs as point features. However, in some cases, VIs could decrease the classification performance. Furthermore, it was found that, on average, the CRF outperforms the ANN for point clouds, yet for low-quality point clouds, the ANN shows better performance.

We inferred the ground points elevation using the point clouds at high quality and feature set that performed the best

TABLE VII
ELEVATION COMPARISON

Point Cloud	Feature set	Elevation difference m	
		Average	Standard Deviation
PC 1.1	Set 3	0.416	0.666
PC 1.2	Set 3	1.210	1.774
PC 2.1	Set 8	0.412	0.634
PC 2.2	Set 2	0.737	0.897

classification results. Furthermore, we compared the estimated DTMs with a reference DTM, which was determined by LAStools software. Table VII shows elevation comparison statistics.

V. DISCUSSION OF RESULTS

In general, the survey data allowed to retrieve a good 3D reconstruction of the study areas. Nevertheless, PC 2.2 has not correctly reconstructed the study area #2. The second survey of the study area #2 has been performed under winds about 10 km h^{-1} . Captured images were blurred. Thus, high- and low-quality reconstruction could not retrieve a fair reconstruction of the study area. Low-quality point cloud was most affected.

Remarkable differences because of point cloud quality take place in the first study area. In particular, the percentage of ground points in PC 1.1 at high- and low-quality are very different (see Table V). We advocated the ground points dissimilarity by light conditions and Agisoft parameter setup. First, the survey was performed at 13:00 GTM-4; thus, the sun was near at the highest point. This lighting might favor photogrammetric reconstruction; there is more contrast between ground and canopy features. Nevertheless, the lighting advantages are lost when Agisoft generates the point cloud at low quality. At low quality, Agisoft uses a downsampled version of the images (for more details, see [19]). Therefore, most of the ground points might be obscured by surrounding canopy points. Note that this phenomenon is not noticed in the remaining surveys because both surveys were taken at low solar angles (see Appendix A).

We found that CRF and GRF are suitable frameworks for generating DTM using multispectral point clouds. In general, CRF models performed better than ANN, specifically when using point clouds at high quality. At first glance, the ANN was better suited to discriminate ground points by low-quality point clouds. Furthermore, lighting conditions or flight altitude do not affect classification accuracy. However, we suggest performing more experiments at different illumination and flight altitudes because they are critical factors in point cloud generation.

Although CRF performed relevant classification results, it is hard to identify a single feature set that best improves the CRF outcomes. In general, CRF best outcomes are achieved by different VIs (see Table VIII). For instance, when using the PC 1.1 at high and low quality, the green normalized difference vegetation index (NDVI) (GNDVI) and modified chlorophyll absorption reflectance index (MCARI) indices are the ones that perform the best results, respectively. However, these

indices do not enhance the performance of other point clouds. Thus, the CRF might yield particular outcomes according to the study area and survey time. Nevertheless, based on CRF performance with high-quality point clouds, we consider that the NDVI, GNDVI, and MCARI could be the most suitable indices for ground filtering in forested regions.

Regarding the CRF performance using low-quality point clouds, it might be explained because of the lack of details between neighbors. As it was mentioned before, downsampled images generate low-quality point clouds. In general, downsampled images have lower details, and the surfaces became smooth. Thus, the CRF might not be able to retrieve enough contextual information from neighboring points. In brief, when using lower-quality point clouds, the CRF could not generate an accurate classification model.

The VIs do not improve the CRF performance. In particular, the PC 2.2 at low quality shows that VIs do not add information for ground identification (see Table VIII). Moreover, PC 2.2 at low quality shows a better classification accuracy than PC 2.2 at high quality. These odd outcomes can be explained by the lousy reconstruction of study area #2 (see Appendix A). Specifically, at low quality, some regions that belong to the canopy were not included in the point cloud because blurred images do not retrieve matching points.

On the other side, in many instances, the inclusion of all VIs in the ANN model outperforms the results of other feature sets. Thus, the feature set 11 (see Table IV), might be considered as the set that enhances ANN performance. Note that ANN achieves a lower classification accuracy than CRF for point clouds at high quality; however, the accuracy difference is not more significant than three percent. Based on classification accuracy, ANN might be suitable for determining a general classification model. The omission errors reported in Table VIII show that ANN is prone to label ground as a canopy. Some omission errors rise to 50%. Furthermore, the commission error standard deviation shows that ANN might be an unstable model for identifying canopy points.

From Table VIII, one also can infer that ANN has better classification accuracy when it is trained and validated using the point clouds at low quality. Note that low-quality point clouds might not retrieve ground points because of image downsampling. Omitted points are the ones surrounded by canopy points (see Appendix A). Moreover, the ANN model is trained using point features, and it does not explore the relationship between neighboring points. Thus, ANN classification metrics might increase because it is a local classification model, and difficult points to classify are excluded.

Both models (CRF, ANN) showed that classification accuracy might be increased by including vegetation features. Moreover, they show that point cloud quality slightly affects the performance of each model. In particular, the classification accuracy is lower than 3%. Here, we do not consider the PC 2.2 due to the imperfect 3-D reconstruction of study area #2. Nevertheless, we suggest using high-quality point clouds because of the information retrieved.

The GRF generates smoother DTM than LAStools. Regarding elevation errors, the lowest error was 0.412 m and the highest 1.210 m. High elevation errors occur for

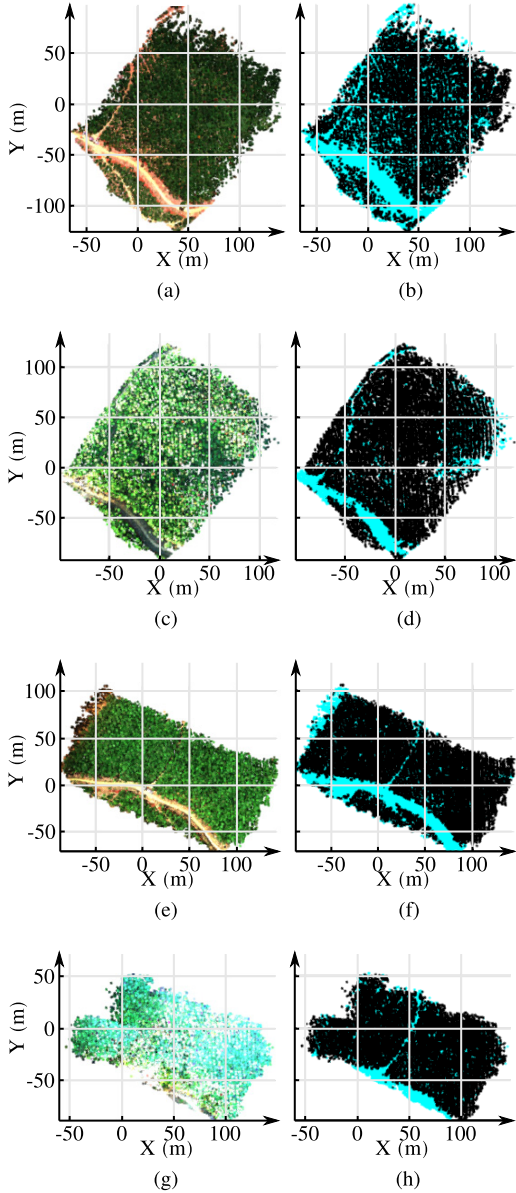


Fig. 3. Point clouds and point labels at high quality from the study areas. Study areas and surveys are described in Section II. For ground labels, black points denote canopy points, and cyan points are ground points. (a) Study area #1, survey 1. (b) Ground labels. (c) Study area #1, survey 2. (d) Ground labels. (e) Study area #2, survey 1. (f) Ground labels. (g) Study area #2, survey 2. (h) Ground labels.

PC 1.2 and PC2.2. These point clouds were generated with data captured at the lowest solar angles. In these cases, the traditional ground filtering method (i.e. LAStools) produces a rougher DTM. LAStools might generate a more complex terrain due to bad ground filtering. Appendix B shows qualitative results for ground elevation models. Based on these results, we inferred that GRF is an advisable framework to estimate ground points occluded by the forest canopy.

In general, we have shown that the CRF model is suitable for discriminating ground points in forested regions. This model can integrate vegetation features (i.e. vegetation indices) as contextual information to enhance classification metrics. In particular, we consider that NDVI, GNDVI, and MCARI are

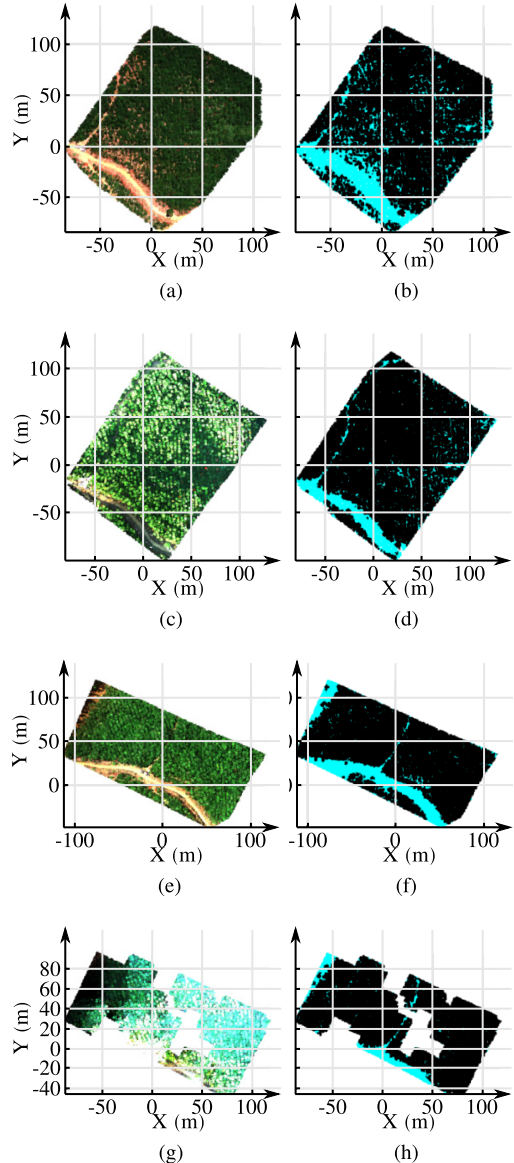


Fig. 4. Point clouds and point labels at low quality from the study areas. Study areas and surveys are described in Section II. For ground labels, black points denote canopy points, and cyan points are ground points. (a) Study area #1, survey 1. (b) Ground labels. (c) Study area #1, survey 2. (d) Ground labels. (e) Study area #2, survey 1. (f) Ground labels. (g) Study area #2, survey 2. (h) Ground labels.

the best suited VIs. Nevertheless, for future works, we suggest assessing larger study areas with different lighting conditions. Moreover, compare the proposed method with airborne LiDAR or Synthetic Aperture Radar. These sensors might retrieve better geometric features. Furthermore, we expect that the characterization of high and low vegetation should increase classification performance.

VI. CONCLUSION

In this work, we evaluated the potential of CRF, ANN, and GRF for the generation of DTMs in forest regions when vegetation features are known. In particular, we computed nine vegetation indices that summarize vegetation and terrain features from a multispectral point cloud. The point clouds

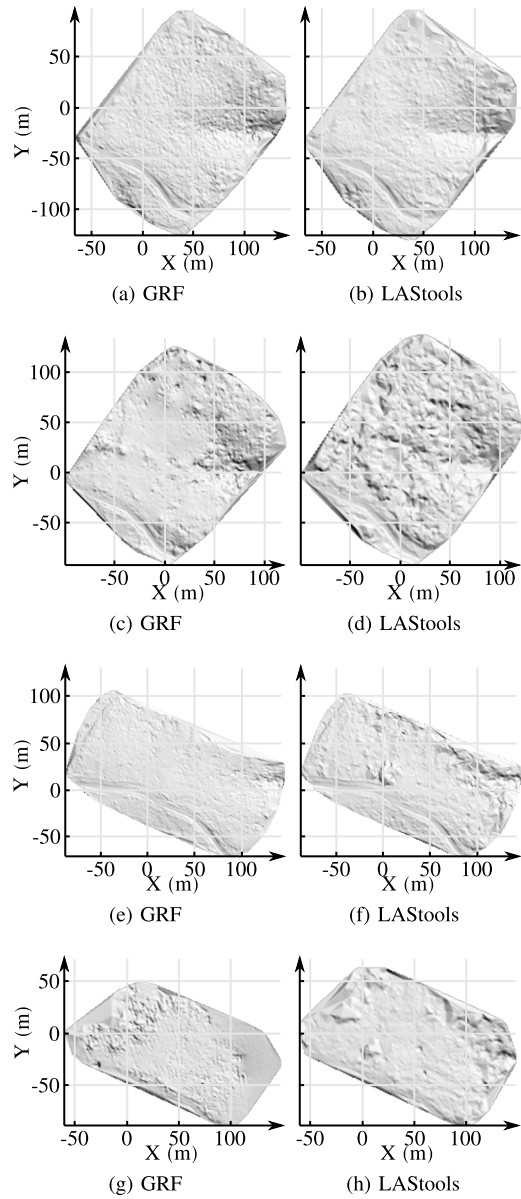


Fig. 5. Digital terrain model of the study areas generated by GRF and LAStools. Study area #1, survey 1: (a) and (b); study area #1, survey 2: (c) and (d); Study area #2, survey 1: (e) and (f); study area #2, survey 2: (g) and (h).

were derived from a photogrammetric RPA surveys performed in Maule, Chile. The CRF and ANN classification models were evaluated by cross-validation procedure. Note that we use different feature input vectors to train the CRF. These feature input vectors allow assessing the behavior of CRF when VI values were incorporated. In general, results showed that VIs enhance classification accuracy. We found that NDVI, GNDVI, and MCARI are the best suited for ground filtering. Nevertheless, they might be site- and time-dependent. Thus, we suggest performing more experiments to determine the most suitable VIs. When the CRF model was compared to ANN models, the former performed best results, and classification accuracy about 87.4% with a standard deviation of 2.9. Nevertheless, in future works, the ANN structure might be modified to perform better results. Regarding the GRF,

TABLE VIII
CROSS-VALIDATION RESULTS OBTAINED USING THE POINT CLOUDS DESCRIBED IN TABLE V AND FEATURE SETS SHOWN IN TABLE IV.
HIGHLIGHTED CELLS SHOW BEST ACCURACY OUTCOMES

Point Cloud	Quality	Feature Set	CRF				ANN			
			<i>om</i>	<i>com</i>	<i>e_{total}</i>	<i>acc</i>	<i>om</i>	<i>com</i>	<i>e_{total}</i>	<i>acc</i>
PC 1.1	High	Set 1	7.93	15.4	12.8	87.2	19.6	14.4	17.3	82.7
		Set 2	7.18	14.6	12.1	87.9	16.9	14.2	14.5	85.5
		Set 3	6.82	14.4	11.6	88.4	16.5	14.6	15.4	84.6
		Set 4	7.09	14.3	11.9	88.1	13.3	18.7	15.1	84.9
		Set 5	7.53	14.3	12.1	87.9	12.8	20.0	16.1	83.9
		Set 6	8.16	13.5	11.9	88.1	14.1	18.2	15.5	84.5
		Set 7	7.67	16.1	13.1	86.9	16.3	16.3	16.2	83.8
		Set 8	7.86	14.2	12.1	87.9	13.4	18.9	15.2	84.8
		Set 9	8.20	14.3	12.5	87.5	17.9	14.2	15.7	84.3
		Set 10	7.85	14.1	12.0	88.0	14.0	25.4	18.2	81.8
		Set 11	7.54	14.0	11.7	88.3	14.2	15.7	14.0	86.0
PC 1.2	Low	Set 1	20.1	14.5	15.5	84.5	22.8	11.2	14.6	85.4
		Set 2	17.2	14.9	14.8	85.2	27.7	7.52	11.7	88.3
		Set 3	17.7	14.5	14.6	85.4	28.9	6.78	11.6	88.4
		Set 4	18.3	13.9	14.3	85.7	27.1	8.24	12.4	87.6
		Set 5	17.4	14.3	14.4	85.6	27.2	7.43	12.3	87.7
		Set 6	18.6	13.7	14.0	86.0	27.2	7.72	12.8	87.2
		Set 7	18.9	13.7	14.2	85.8	28.6	7.33	12.7	87.3
		Set 8	19.1	13.1	13.7	86.3	28.7	7.15	12.6	87.4
		Set 9	18.4	14.9	15.3	84.7	30.7	5.99	11.8	88.2
		Set 10	18.3	13.7	14.2	85.8	31.9	5.34	11.9	88.1
		Set 11	17.0	15.4	15.0	85.0	27.8	6.57	11.4	88.6
PC 2.1	High	Set 1	34.7	10.4	16.1	83.9	46.5	5.87	15.0	85.0
		Set 2	41.0	7.33	15.7	84.3	49.3	4.55	14.3	85.7
		Set 3	29.6	9.26	13.4	86.6	54.9	3.92	16.0	84.0
		Set 4	42.7	10.4	21.3	78.7	48.9	4.89	14.7	85.3
		Set 5	29.1	9.73	14.7	85.3	46.0	5.28	14.7	85.3
		Set 6	25.0	13.5	17.1	82.9	45.6	5.71	15.4	84.6
		Set 7	21.6	11.9	14.6	85.4	57.4	4.57	17.2	82.8
		Set 8	17.1	16.0	17.5	82.5	43.5	8.42	17.1	82.9
		Set 9	24.4	12.2	16.6	83.4	45.2	6.14	14.9	85.1
		Set 10	21.7	13.8	16.6	83.4	50.0	7.51	18.6	81.4
		Set 11	20.5	11.1	14.0	86.0	55.5	2.01	13.5	86.5
PC 2.2	Low	Set 1	28.6	11.7	15.1	84.9	39.8	6.37	12.9	87.1
		Set 2	26.0	11.7	14.6	85.4	38.9	5.48	12.1	87.9
		Set 3	25.9	13.8	16.3	83.7	38.9	5.96	12.6	87.4
		Set 4	38.6	10.5	15.2	84.8	38.4	6.79	13.3	86.7
		Set 5	16.5	15.4	16.0	84.0	37.9	6.28	13.0	87.0
		Set 6	17.3	15.6	16.1	83.9	37.3	6.64	13.1	86.9
		Set 7	25.0	16.3	18.0	82.0	40.7	5.55	12.7	87.3
		Set 8	13.5	17.4	16.9	83.1	40.0	5.70	12.6	87.4
		Set 9	24.4	14.2	16.3	83.7	39.4	6.23	12.8	87.2
		Set 10	25.9	13.4	16.0	84.0	40.3	6.07	12.9	87.1
		Set 11	16.6	13.6	14.5	85.5	39.8	5.12	12.5	87.5
PC 2.1	High	Set 1	9.57	7.58	8.80	91.2	17.5	9.80	12.2	87.8
		Set 2	8.21	8.41	9.12	90.9	13.2	6.85	7.02	93.0
		Set 3	9.76	7.35	8.51	91.5	16.9	7.46	8.40	91.6
		Set 4	10.5	6.31	8.20	91.8	17.3	6.34	7.40	92.6
		Set 5	14.7	9.10	10.7	89.3	17.0	6.16	7.27	92.7
		Set 6	10.5	6.02	8.07	91.9	16.6	6.24	6.94	93.1
		Set 7	10.6	6.89	8.75	91.3	13.4	9.85	9.63	90.4
		Set 8	9.58	6.02	7.94	92.1	14.3	8.37	7.62	92.4
		Set 9	10.3	8.07	9.41	90.6	19.9	5.45	8.60	91.4
		Set 10	11.3	7.37	9.46	90.5	15.0	8.36	8.95	91.0
		Set 11	8.71	7.72	8.83	91.2	15.6	6.84	6.75	93.2
PC 2.2	Low	Set 1	12.8	10.3	10.2	89.8	26.8	7.30	10.5	89.5
		Set 2	23.2	9.11	12.6	87.4	25.9	4.08	7.77	92.2
		Set 3	11.5	11.3	10.9	89.1	26.6	4.61	8.47	91.5
		Set 4	11.9	9.72	9.47	90.5	26.5	4.48	8.20	91.8
		Set 5	12.0	9.53	9.40	90.6	25.9	4.18	7.64	92.4
		Set 6	12.3	9.26	9.30	90.7	27.3	4.51	8.27	91.7
		Set 7	27.7	8.81	13.5	86.5	28.9	4.92	9.04	91.0
		Set 8	24.4	8.76	12.6	87.4	27.7	4.44	8.27	91.7
		Set 9	14.8	10.9	11.3	88.7	27.5	4.56	8.71	91.3
		Set 10	13.7	9.77	10.2	89.8	27.1	4.64	8.69	91.3
		Set 11	11.6	9.45	9.67	90.3	26.1	3.95	7.54	92.5
PC 2.1	High	Set 1	5.81	17.6	15.7	84.3	22.0	36.1	31.2	68.8
		Set 2	7.59	8.77	8.60	91.4	19.4	36.4	30.1	69.9
		Set 3	8.14	12.9	12.1	87.9	15.7	39.8	32.6	67.4
		Set 4	8.08	10.3	10.1	89.9	24.3	19.9	20.0	80.0
		Set 5	4.51	9.54	8.68	91.3	17.8	23.1	21.8	78.2
		Set 6	5.82	15.2	13.9	86.1	19.3	32.8	27.6	72.4
		Set 7	20.7	12.4	16.7	83.3	15.5	23.5	20.9	79.1
		Set 8	8.17	13.6	14.1	85.9	20.0	22.4	21.2	78.8
		Set 9	10.7	10.7	10.9	89.1	18.0	48.2	39.1	60.9
		Set 10	10.4	12.9	11.8	88.2	23.6	26.8	24.4	75.6
		Set 11	4.58	9.77	9.03	91.0	17.9	27.1	22.8	77.2
PC 2.2	Low	Set 1	9.73	7.92	7.99	92.0	31.3	5.35	9.04	91.0
		Set 2	16.2	7.95	9.73	90.3	30.7	3.44	7.02	93.0
		Set 3	8.78	10.0	9.95	90.0	31.6	4.76	8.56	91.4
		Set 4	26.3	7.24	9.63	90.4	27.0	8.07	10.5	89.5
		Set 5	19.5	9.07	11.5	88.5	28.3	8.70	11.4	88.6
		Set 6	26.4	8.45	10.9	89.1	35.3	5.45	9.71	90.3
		Set 7	38.7	5.13	10.5	89.5	25.6	9.06	11.2	88.8
		Set 8	24.3	8.82	11.1	88.9	36.7	4.90	9.41	90.6
		Set 9	7.39	10.5	10.1	89.9	31.4	5.67	9.27	90.7
		Set 10	21.9	12.0	14.3	85.7	30.6	5.26	8.74	91.3
		Set 11	26.7	8.49	11.5	88.5	26.5	4.01	6.91	93.1

it generates more smoothed DTMs than LAStools. When using data at low solar angles, LAStools might fail to filter ground points.

APPENDIX A POINT CLOUDS AT HIGH- AND LOW-QUALITY FOR EACH STUDY AREA AND SURVEY

See Figs. 3 and 4.

APPENDIX B DIGITAL TERRAIN MODELS: QUALITATIVE RESULTS

See Fig. 5.

APPENDIX C CROSS-VALIDATION RESULTS

See Table VIII.

REFERENCES

- [1] (2020). CONAF. [Online]. Available: <http://www.conaf.cl/incendios-forestales/incendios-forestales-en-chile/estadisticas-historicas/>
- [2] F. de la Barrera, F. Barraza, P. Favier, V. Ruiz, and J. Quense, "Megafires in Chile 2017: Monitoring multiscale environmental impacts of burned ecosystems," *Sci. Total Environ.*, vols. 637–638, pp. 1526–1536, Oct. 2018, doi: [10.1016/j.scitotenv.2018.05.119](https://doi.org/10.1016/j.scitotenv.2018.05.119).
- [3] M. C. Soto, G. Julio-Alvear, and R. G. Salinas, "Current wildfire risk status and forecast in Chile: Progress and future challenges," in *Wildfire Hazards, Risks and Disasters*. Amsterdam, The Netherlands: Elsevier, 2015, pp. 59–75.
- [4] P. Tarolli, "High-resolution topography for understanding Earth surface processes: Opportunities and challenges," *Geomorphology*, vol. 216, pp. 295–312, Jul. 2014, doi: [10.1016/j.geomorph.2014.03.008](https://doi.org/10.1016/j.geomorph.2014.03.008).
- [5] J. Niemeyer, F. Rottensteiner, U. Soergel, and C. Heipke, "Contextual classification of point clouds using a two-stage CRF," *Int. Arch. Photogramm., Remote Sens. Spatial Inf. Sci.*, vol. 40, no. 3W2, pp. 141–148, 2015.
- [6] Z. Chen, B. Gao, and B. Devereux, "State-of-the-art: DTM generation using airborne LiDAR data," *Sensors*, vol. 17, no. 12, p. 150, Jan. 2017.
- [7] M. Ceanu and C. Arcadie, "ALS for terrain mapping in forest environments: An analysis of LiDAR filtering algorithms," *EARSel eProceedings*, vol. 16, no. 1, pp. 9–20, 2017.
- [8] F. Bretar and N. Chehata, "Terrain modeling from LiDAR range data in natural landscapes: A predictive and Bayesian framework," *IEEE Trans. Geosci. Remote Sens.*, vol. 48, no. 3, pp. 1568–1578, Mar. 2010.
- [9] M. J. Westoby, J. Brasington, N. F. Glasser, M. J. Hambrey, and J. M. Reynolds, "Structure-from-motion" photogrammetry: A low-cost, effective tool for geoscience applications," *Geomorphology*, vol. 179, pp. 300–314, Dec. 2012, doi: [10.1016/j.geomorph.2012.08.021](https://doi.org/10.1016/j.geomorph.2012.08.021).
- [10] A. Graham, N. Coops, M. Wilcox, and A. Plowright, "Evaluation of ground surface models derived from unmanned aerial systems with digital aerial photogrammetry in a disturbed conifer forest," *Remote Sens.*, vol. 11, no. 1, p. 84, Jan. 2019.
- [11] J. Jensen and A. Mathews, "Assessment of image-based point cloud products to generate a bare Earth surface and estimate canopy heights in a woodland ecosystem," *Remote Sens.*, vol. 8, no. 1, p. 50, Jan. 2016.
- [12] X. Meng *et al.*, "Photogrammetric UAV mapping of terrain under dense coastal vegetation: An object-oriented classification ensemble algorithm for classification and terrain correction," *Remote Sens.*, vol. 9, no. 11, pp. 1–23, 2017.
- [13] M. Isenburg, H. Trunzer, F. Malmer, A. Aerospace, S. Limited, and C. P. Bldg, "Experiences with LiDAR canopy penetration," in *Proc. 35th Asian Conf. Remote Sens. (ACRS)*. AARS, 2014, pp. 228–234.
- [14] S. A. Gilani, M. Awrangjeb, and G. Lu, "Fusion of LiDAR data and multispectral imagery for effective building detection based on graph and connected component analysis," *Int. Arch. Photogramm., Remote Sens. Spatial Inf. Sci.*, vol. 40, no. 3W2, pp. 65–72, 2015.
- [15] N. Anders, J. Valente, R. Masselink, and S. Keesstra, "Comparing filtering techniques for removing vegetation from UAV-based photogrammetric point clouds," *Drones*, vol. 3, no. 3, p. 61, Jul. 2019.
- [16] W. L. Lu, K. P. Murphy, J. J. Little, A. Sheffer, and H. Fu, "A hybrid conditional random field for estimating the underlying ground surface from airborne LiDAR data," *IEEE Trans. Geosci. Remote Sens.*, vol. 47, no. 8, pp. 2913–2922, Aug. 2009.
- [17] BCN B. (Jun. 2020). *Clima y Vegetación Región de Valparaíso*. [Online]. Available: <https://www.bcn.cl/siit/nuestropais/region5/clima.htm>
- [18] J. Frey, K. Kovach, S. Stemmler, and B. Koch, "UAV photogrammetry of forests as a vulnerable process. A sensitivity analysis for a structure from motion RGB-image pipeline," *Remote Sens.*, vol. 10, no. 6, p. 912, Jun. 2018.
- [19] M. Agisoft. (Jun. 2020). *Micasense Rededge MX Processing Workflow (Including Reflectance Calibration) in Agisoft Metashape Professional 1.5*. [Online]. Available: <https://agisoft.freshdesk.com/support/solutions/articles/31000148780-micasense-rededge-mx-processing-workflow-including-reflectance-calibration-in-agisoft-metashape-pro>
- [20] MicaSense. (Jun. 2021). *Rededge Camera Radiometric Calibration Model*. [Online]. Available: <https://support.micasense.com/hc/en-us/articles/115000351194-RedEdge-Camera-Radiometric-Calibration-Models>
- [21] J. T. Pingel, C. K. Clarke, and A. W. McBride, "An improved simple morphological filter for the terrain classification of airborne LiDAR data," *ISPRS J. Photogram. Remote Sens.*, vol. 77, pp. 21–30, Mar. 2013.
- [22] M. Isenburg. *Lastools—Efficient LiDAR Processing Software (Version 191018, Unlicensed)*. Accessed: Jan. 7, 2021. [Online]. Available: <https://rapidlasso.com/lastools/>
- [23] M. Schmidt. (2007). *UGM: A MATLAB Toolbox for Probabilistic Undirected Graphical Models*. [Online]. Available: <http://www.cs.ubc.ca/schmidtm/Software/UGM.html>
- [24] K. P. Murphy, *Machine Learning: A Probabilistic Perspective*. Cambridge, MA, USA: MIT Press, 2012.
- [25] T. Arevalo-Ramirez and F. A. Cheein, "Conditional random field features and structure assessment for digital terrain modeling," *IEEE Access*, vol. 9, pp. 37146–37155, 2021.
- [26] S. Jin, Y. Su, X. Zhao, T. Hu, and Q. Guo, "A point-based fully convolutional neural network for airborne LiDAR ground point filtering in forested environments," *IEEE J. Sel. Topics Appl. Earth Observ. Remote Sens.*, vol. 13, pp. 3958–3974, Jul. 2020.
- [27] N. Viljanen, E. Honkavaara, R. Näsi, T. Hakala, O. Niemeläinen, and J. Kaivosoja, "A novel machine learning method for estimating biomass of grass swards using a photogrammetric canopy height model, images and vegetation indices captured by a drone," *Agriculture*, vol. 8, no. 5, p. 70, May 2018.
- [28] J. W. Rouse, R. H. Haas, J. A. Schell, D. W. Deering, and J. C. Harlan, "Monitoring the vernal advancement and retrogradation (green wave effect) of natural vegetation," Greenbelt, MD, USA, NASA/GSFC Type III Final Rep., 1974, vol. 371.
- [29] A. Gitelson, Y. J. Kaufman, and M. N. Merzlyak, "Use of a green channel in remote sensing of global vegetation from EOS-MODIS," *Remote Sens. Environ.*, vol. 58, no. 3, pp. 289–298, 1996.
- [30] J. Qi, A. Chehbouni, A. R. Huete, Y. H. Kerr, and S. Sorooshian, "A modified soil adjusted vegetation index," *Remote Sens. Environ.*, vol. 48, no. 2, pp. 119–126, 1994.
- [31] G. Rondeaux, M. Steven, and F. Baret, "Optimization of soil-adjusted vegetation indices," *Remote Sens. Environ.*, vol. 55, no. 2, pp. 95–107, 1996.
- [32] A. R. Huete, K. Didan, T. Miura, E. P. Rodriguez, X. Gao, and L. G. Ferreira, "Overview of the radiometric and biophysical performance of the MODIS vegetation indices," *Remote Sens. Environ.*, vol. 83, nos. 1–2, pp. 195–213, 2002.
- [33] M. S. Kim, "The use of narrow spectral bands for improving remote sensing estimations of fractionally absorbed photosynthetically active radiation," Ph.D. dissertation, Dept. Geography, Univ. Maryland, College Park, MD, USA, 1994.
- [34] C. S. T. Daughtry, C. L. Walthall, M. S. Kim, E. B. de Colstoun, and J. E. McMurtrey, III, "Estimating corn leaf chlorophyll concentration from leaf and canopy reflectance," *Remote Sens. Environ.*, vol. 74, no. 2, pp. 229–239, 2000.
- [35] C. Wu, Z. Niu, Q. Tang, and W. Huang, "Estimating chlorophyll content from hyperspectral vegetation indices: Modeling and validation," *Agricul. Forest Meteorol.*, vol. 148, nos. 8–9, pp. 1230–1241, 2008.



Tito Arevalo-Ramirez was born in Loja Ecuador in 1992. He received the B.S. degree in electronic and control engineering from Escuela Politécnica Nacional (EPN), Quito, Ecuador, in 2016. He is currently pursuing the Ph.D. degree in electronic engineering with Universidad Técnica Federico Santa María (UTFSM), Valparaíso, Chile.

From 2015 to 2018, he was involved in research duties in EPN and Universidad Técnica de Machala, Machala, Ecuador. His research interests include machine learning, remote sensing, robotics, agriculture, and forestry.



Javier Guevara (Member, IEEE) received the B.S. degree in electronics and control engineering from Escuela Politécnica Nacional Quito, Ecuador, in 2016, and the Ph.D. degree from Universidad Técnica Federico Santa María, Valparaíso, Chile, in 2021.

He is currently working as Post-Doctoral Researcher with the University of California at Davis, Davis, CA, USA. His research interests include plant phenotyping, 3-D modelling, sensor fusion, artificial intelligence, and mobile robotics.



Andrés Fuentes is a Full Professor with the Departamento de Industrias, Universidad Técnica Federico Santa María, Valparaíso, Chile. The teaching focuses on the fundamentals of energy, fluid mechanics, heat transfer and combustion. The research is carried out in the Energy Conversion and Combustion Group (EC2G) working mainly in experiments based in bench-scale set-ups, applying non-intrusive optical laser-based diagnostics and numerical simulation in combustion and their environmental issues for conventional and renewable fuels, ignition and propagation of forest fires and thermal solar energy.



Robert Guaman Rivera was born in Loja Ecuador, in 1989. He received the B.S. degree in electronic and control engineering from Escuela Politécnica Nacional (EPN), Quito, Ecuador, in 2016. He is currently pursuing the Ph.D. degree in electronic engineering with the Universidad Técnica Federico Santa María, Valparaíso, Chile.

His research interests include control systems, path planning, mobile manipulation, machine learning, smart agriculture, robotics, automation in construction, and 3-D concrete printing.



Juan Villacréz received the B.S. degree in electronic and control engineering from Escuela Politécnica Nacional, Quito, Ecuador, in 2016. He is currently pursuing the Ph.D. degree in electronic engineering with Universidad Técnica Federico Santa María, Valparaíso, Chile.

His research interest comprises several aspects of robotics, perception in agriculture, and image processing.



Fernando Auat Cheein (Senior Member, IEEE) received the B.S. degree in electronics engineering from the Universidad Nacional de Tucumán, Tucumán, Argentina, in 2002, and the M.S. and Ph.D. degrees in control systems from the Universidad Nacional de San Juan, San Juan, Argentina, in 2005 and 2009, respectively.

Since 2011, he has been an Assistant Professor with the Department of Electronic Engineering, Universidad Técnica Federico Santa María, Valparaíso, Chile. He is also the Founder of the Autonomous

and Industrial Robotics Research Group (GRAI) and part of the board of the Advanced Center for Electrical and Electronic Engineering, Chile. He has authored three book chapters and has published 27 journal articles. His research interests include autonomous navigation, agricultural robotics, and estimation theory.

Dr. Auat Cheein received the International Joint Conference on Biomedical Engineering Systems and Technologies Best Paper Award in 2008, Best National Innovation/Technology Development Award granted by the Institute of Electrical and Electronics Engineers in Chile in 2015, and the Outstanding Teaching Award granted by Universidad Técnica Federico Santa María, from 2012 to 2014.



Oswaldo Menéndez (Member, IEEE) was born in Quito, Ecuador. He received the bachelor's degree in electronic engineering from Escuela Politécnica Nacional Quito, Ecuador, in 2013, and the Ph.D. degree in electronic engineering from Universidad Técnica Federico Santa María, Valparaíso, Chile, in 2019.

He is currently a Post-Doctoral Researcher with the Advanced Center for Electric and Electronic Engineering, Universidad Técnica Federico Santa María. His main research areas are focused on energy harvesting technologies, robotics in power systems, and automated inspection systems.